### Title

Low Wall Shear Stress Is Associated with Saphenous Vein Graft Stenosis in Patients with Coronary Artery Bypass Grafting




### Journal

Journal of Cardiovascular Translational Research, 14(4)

### ISSN

1937-5387



### Authors

Khan, Muhammad Owais
Tran, Justin S
Zhu, Han
et al.



### Publication Date

2021-08-01

### DOI

10.1007/s12265-020-09982-7

Peer reviewed

HHS Public Access

Author manuscript

*J Cardiovasc Transl Res*. Author manuscript; available in PMC 2022 August 01.

Published in final edited form as:

*J Cardiovasc Transl Res*. 2021 August ; 14(4): 770–781. doi:10.1007/s12265-020-09982-7.

# Low Wall Shear Stress is Associated with Saphenous Vein Graft Stenosis in Patients with Coronary Artery Bypass Grafting

**Muhammad Owais Khan, Ph.D.**[1,2], **Justin S. Tran, Ph.D.**[3], **Han Zhu, M.D.**[4], **Jack Boyd, M.D.**[5], **René R. Sevag Packard, M.D., Ph.D.**[6], **Ronald P. Karlsberg, M.D.**[7], **Andrew M. Kahn, M.D., Ph.D.**[8], **Alison L. Marsden, Ph.D.**[1,2,9,10]

[1]Department of Pediatrics, Stanford University School of Medicine, Stanford, California.

[2]Institute for Computational and Mathematical Engineering, Stanford University, Stanford, California.

[3]Department of Mechanical Engineering, California State University Fullerton, Fullerton, California.

[4]Department of Cardiovascular Medicine, Stanford University School of Medicine, Stanford, California.

[5]Department of Cardiothoracic Surgery, Stanford University School of Medicine, Stanford, California.

[6]Department of Medicine, University of California Los Angeles, Los Angeles, California.

[7]Cardiovascular Medical Group of Southern California, Beverly Hills, California.

[8]Division of Cardiovascular Medicine, University of California San Diego, La Jolla, California.

[9]Department of Bioengineering, Stanford University, Stanford, California.

[10]Stanford Cardiovascular Institute, Stanford University, Stanford, California.

## Abstract

Biomechanical forces may play a key role in saphenous vein graft disease (SVG) disease after coronary artery bypass graft (CABG) surgery. Computed Tomography Angiography (CTA) of 430



**Corresponding Author:** Name: Alison L. Marsden, amarsden@stanford.edu, Address: 318 Campus Drive, E1.3, Stanford, California, 94305-5428, Tel: 650-723-7739, Name: **Andrew Kahn**, akahn@ucsd.edu, Address: UCSD Sulpizio Cardiovascular Center, 9452 Medical Center Dr., # 7411, La Jolla, California, 92037-7411, Tel: 858-246-2989.



DISCLOSURES

None

HUMAN SUBJECTS/INFORMED CONSENT STATEMENT

All procedures followed were in accordance with the ethical standards of the responsible committee on human experimentation (institutional and national) and with the Helsinki Declaration of 1975, as revised in 2000 (5). Informed consent was obtained from all patients for being included in the study. No animal studies were carried out by the authors for this article. Patient recruitment and access to non-invasive clinical data (computer tomographic (CT) images, echocardiography data) was carried out according to protocols approved by the Stanford University Institutional Review Board.

post-CABG patients were evaluated and 15 patients were identified with both stenosed and healthy SVGs for paired analysis. The stenosis was virtually removed, and detailed 3D models were reconstructed to perform patient-specific computational fluid dynamic (CFD) simulations. Models were processed to compute anatomic parameters, and hemodynamic parameters such as local and vessel-averaged wall shear stress (WSS), normalized WSS (WSS*), low shear area (LSA), oscillatory shear index (OSI) and flow rate. WSS* was significantly lower in pre-diseased SVG segments compared to corresponding control segments without disease (1.22 vs. 1.73, p=0.012) and the area under the ROC curve was 0.71. No differences were observed in vessel-averaged anatomic or hemodynamic parameters between pre-stenosed and control whole SVGs. There are currently no clinically available tools to predict SVG failure post-CABG. CFD modelling has the potential to identify high-risk CABG patients who may benefit from more aggressive medical therapy and closer surveillance.

### Keywords

Computational fluid dynamics; coronary artery bypass graft surgery; saphenous vein graft; wall shear stress; computed tomography angiography

## INTRODUCTION

Coronary artery bypass grafting (CABG) is the most commonly performed cardiac surgical procedure worldwide, with > 150,000 surgeries performed annually in the US[1]. Though CABG improves symptoms and survival in patients with diffuse, multi-vessel obstructive coronary artery disease, long term surgical success depends on continued graft patency. While the internal mammary artery is the preferred choice for revascularization of the left anterior descending artery (LAD), saphenous vein grafts (SVGs) are commonly used owing to availability and length in about 70% of CABG surgeries[2]. However, SVGs continue to be plagued by poor long-term patency. Recent follow-up from the PREVENT IV trial showed that only 75% of SVGs remained free from severe stenoses or obstruction at 12 to 18 months[3]. SVG patency is severely reduced at 10-year follow-up, with patency rates of 55% to 60%[2]. SVG occlusion is often silent and underdiagnosed, and associated with poor long-term outcomes. Once occluded, SVGs can be challenging for percutaneous interventions and repeat surgical revascularization is associated with increased morbidity and mortality, making SVG failure a significant clinical challenge[4].

Biomechanical forces are known to influence the complex, multifactorial arterialization and remodelling process of SVGs following implantation into the systemic circulation[5]. However, the mechanobiological processes leading to favorable remodeling and arterialization in some SVGs while leading to maladaptation and atherosclerotic disease, including stenosis and occlusion, in others remain poorly understood. The observation that focal intimal hyperplasia and stenotic atherosclerosis lesions are typically “site specific” portends an interaction between disturbed flow in susceptible regions and disease pathogenesis. Numerous in-vitro studies have shown that low and oscillatory wall shear stress (WSS) predispose endothelial cells to atherosclerosis[6]; however, these hemodynamic forces are typically unattainable from standard clinical imaging modalities for coronary

vessels and bypass grafts, though recent advanced imaging such as 4D Flow MRI has been used to obtain hemodynamics forces and approximations of WSS in larger vessels[7].

Computational fluid dynamics (CFD) has emerged as a promising tool to non-invasively evaluate hemodynamics, investigate disease pathophysiology, develop predictive models of disease progression, and improve treatment strategies[8]. Recent studies have demonstrated the clinical value of simulations based on computed tomographic angiography (CTA) to predict fractional flow reserve ($FFR_{CT}$) in native coronary arteries[9,10]. However, the clinical value of applying similar approaches to CABG has not yet been realized. Recent studies have addressed modelling challenges specific to CABG, including varying tissue properties and realistic models of coronary physiology. These studies have made significant progress towards robust, automated patient-specific CFD simulations in CABG patients[11–13].

The primary goal of this study was to investigate the association between abnormal shear stresses and SVG failure using patient-specific and multi-scale CFD methods. The secondary goal was to investigate novel anatomic parameters to characterize SVG morphology that may be associated with SVG failure. We hypothesized that regions that develop stenosis in SVGs would be predisposed to low wall shear stresses (WSS) compared to regions that remained patent. Accordingly, we retrospectively studied CFD-derived hemodynamic and anatomic parameters in patients with clinically significant SVG stenoses.

## METHODS

### Study Population

We retrospectively reviewed the patient database at the Cardiovascular Medical Group of Southern California between 2005–2016 to identify all post-CABG patients who had undergone subsequent coronary CTA and echocardiography and identified a cohort of 15 patients from a total of N=430 patients. Patients were included in the study if they had at least one moderate-to severely stenosed (defined as ≥ 50% area reduction) or stented SVG and at least one non-stenosed and widely patent SVG at the time of CTA. This allowed patients to serve as their own control. Exclusion criteria included: i) patients with only a single SVG, ii) SVGs that were aneurysmal, iii) patients whose CTA showed significant motion or were otherwise of poor quality. The majority of the patient exclusions was attributed to criteria (i), in which there were diseased SVGs but no control SVGs were present. Applying the aforementioned inclusion and exclusion criteria, a cohort of N=15 CABG patients were included in the study. For the remainder of the manuscript, we refer to stenosed or stented SVGs as “diseased” and non-stenosed widely-patent SVGs as “controls”.

### Image Segmentation, Model Reconstruction and Mesh Generation

Three-dimensional patient-specific anatomic CABG models of the 15 patients were segmented from CTA images using the open-source SimVascular software (www.simvascular.org). The CTA images consisted of 350–400 images with 512 × 512 pixels, an in-plane resolution of 0.39 mm and a slice thickness of 0.625mm. A trained radiology technologist performed all segmentations in 3D and Quantitative Imaging Laboratory at Stanford University (www.3dqlab.stanford.edu), and was blinded to the goal

of the study. Details of the segmentation and reconstruction methodology have previously been described[13]. Briefly, we identified vessel centerlines along the coronary arteries, aorta, aortic branch vessels and bypass grafts. Lumens were segmented on 2D slices perpendicular to the centerline and lofted together to generate a 3D patient-specific anatomic model.

Since immediate post-operative images are not available as a standard-of-care, for each stenosed SVG we virtually removed the stenosis to approximate the pre-stenosed state of the SVG (Figure 1A, 1B). Similarly, in the case of SVGs with stents, we virtually removed the stent. In SimVascular, we identified lumen shapes one vessel-diameter proximal and distal to the stenosis, which were then linearly interpolated to reconstruct the pre-stenosed shape of the vessel. The locations of these stenotic sections were tracked for subsequent stenosis-only analysis.

Reconstructed models were discretized into linear tetrahedral elements using MeshSim (Simmetrix Inc., Clifton Park, NY) for CFD simulations. Three boundary layers and variable mesh resolution were assigned. The following resolutions provided mesh-independent hemodynamic quantities in two representative patients and thus, were applied to the entire cohort: 0.3cm to aorta and aortic branch vessels, 0.035cm to the native coronaries and 0.02cm to the SVGs. The average mesh size was 4.4 million tetrahedral elements ranging from 3.1 to 6.3 million elements, reflecting the variability in SVG and native coronary sizes and extent of CFD model domain.

## Anatomic Parameters Calculation

Three-dimensional models segmented from CTA data were processed to automatically compute SVG anatomic parameters using the *Vascular Modelling Toolkit* (www.vmtk.org). We computed curvature, tortuosity, length and area by discretizing the SVG centerline into 200 equidistant points, which allowed for accurate quantification of the vessel centerline-derived anatomic parameters (Figure 1C). Since cross-sectional area mismatch has previously been proposed as a predictor of SVG failure[14], we also computed the ratio of cross-sectional SVG area to target coronary vessel area.

## Multi-Scale Computational Fluid Dynamics Simulations

Details of the simulation methodology have previously been reported by our group[13]. Briefly, we conducted fluid-structure interaction (FSI) simulations, coupled with lumped parameter network (LPN) boundary conditions to capture the heart and closed-loop circulation. The vessel material properties for aorta, native coronary, SVGs and left/right internal mammary arteries were assigned based on literature values, and were $7\times10^6$, $11.5\times10^6$, $5\times10^6$, and $11.5\times10^6$ dynes/cm$^2$, respectively. Similarly, the wall thickness was approximated to be 10% of the vessel diameter, consistent with published morphometric correlations[15]. Circulation outside of the 3D domain, including the heart, systemic circulation, and microcirculation, was modelled using a closed-loop LPN (Figure 2D). The LPN was designed to model the out-of-phase behavior of coronary flow and pressure waveforms caused by variation in coronary resistance with cardiac contraction, not possible through a standard Windkessel model. For each patient, an automated tuning framework was employed to tune the LPN parameters to match standard-of-care clinical measurements,

including heart rate, systolic and diastolic blood pressure, and left ventricle ejection fraction and cardiac output as measured by echocardiography[12]. We assumed 4% of the total cardiac output went to the coronary arteries, with 70% – 30% flow split to the left and the right coronary tree, respectively[16]. Within each anatomic model, the flow was further distributed to each vessel using a modified Murray's Law that describes a mathematical correlation between vessel size and flow. Specifically, the capacitance values were chosen to be proportional to outlet area, while resistance values were defined using an exponent of 2.0 for aortic branches[17] and 2.66 for the coronary branches[18]. All simulations were run for six cycles to wash out initial transients and 1,000 time-steps were used per cardiac cycle. The final cardiac cycle was used to process hemodynamic quantities.

Simulation results were post-processed to compute parameters of presumed biological relevance (Table 1). Coronary boundary conditions were based on standard morphometric assumptions, which are typically valid in normal conditions. However, in CABG patients, collateral flow or prior infarction can introduce uncertainties in absolute WSS predictions. Thus, to suppress the effect of this uncertainty, we normalized the CFD-derived WSS by the analytical solution for WSS in a straight cylinder of equal diameter and flow (WSS*). Regions of low shear stresses and disturbed flow have also been implicated in vascular diseases (e.g. atherosclerosis) and were estimated using low shear area (LSA) and oscillatory shear index (OSI), respectively. LSA, defined as vessel area exposed to low WSS, has previously been proposed as a plausible biomarker of vascular disease (e.g. atherosclerosis). Although in-vitro studies have shown < 4 dynes/cm$^2$ as a feasible threshold[6], an unequivocal cut-off value has not been established. Thus, we computed regions exposed to WSS below 10, 7.5 and 5, 2.5 dynes/cm$^2$, but found no difference between diseased and control SVGs. Since SVG flow rate is dependent on the target coronary vessel being perfused, large variability could exist in WSS values. To overcome this challenge, we instead defined a graft-level threshold for each SVG. We computed regions exposed to <10% of the averaged WSS in that SVG, which was termed LSA* (Table 1). Flow rates through each SVG were also computed. Based on these processed data, two analyses were performed:

**a.** Comparison of diseased SVG segments (after virtual removal of stenosis/stent) to control segments in non-diseased SVGs within the same patient.

**b.** Comparison of whole diseased SVG to whole non-diseased SVG in the same patient. The control SVG segments were identified at the same normalized distance from the proximal anastomosis as the stenosed segment in the diseased SVG. The control segment was the same normalized length as the diseased segment. The process was repeated in patients with multiple stenoses.

## Statistical Analysis

Statistical analysis was performed on anatomic and hemodynamic parameters to identify the difference between diseased vs. control SVG segments, and diseased vs. control whole SVGs. A Shapiro-Wilk test was performed to check for normality. Since all anatomic and hemodynamic variables were found to be non-normally distributed, a two-sided paired Wilcoxon signed ranksum test was used, and results were reported as median and interquartile range (IQR). Some patients had ≥ 1 control SVGs. Therefore, each diseased

SVG was paired with a randomly selected control SVG such that all pairs were independent. The process was repeated 200 times, and the mean p-value and confidence intervals were calculated. Repeating the random selections 400 times did not show differences. In the analysis, p-values < 0.05 were considered statistically significant. Receiver operating characteristics (ROC) analysis was performed on all parameters to determine the optimal thresholds separating diseased and control SVG segments and diseased and control whole SVGs. Area under the ROC curve (AUC) was computed for each parameter.

## RESULTS

The study population consisted of N=15 patients who have a total of 40 SVGs. On average, patients had 2.7 SVGs and were predominantly men (93%) with a history of hypertension, hyperlipidemia, and prior myocardial infarction (Table 2). There was a total of 40 SVGs: 17 diseased and 23 controls. Because some SVGs had multiple stenoses, there were 28 stenosed/stented segments. The majority of the SVGs were grafted to the obtuse marginal (OM) (43%) followed by the right coronary artery (RCA) (30%) (Table 3).

### Differences in Hemodynamic and Anatomic Parameters

Comparing diseased and control SVG segments, WSS* was significantly lower in diseased segments than in control segments (p=0.012); other quantities, such as curvature, area, WSS and OSI were not significantly different (Table 4). These quantitative values are consistent with the qualitative paired plots shown in Figure 2. WSS* had an AUC value of 0.71, the highest among all parameters investigated. Using an optimal cut-off value of 1.29, the sensitivity and specificity of WSS* were 71% and 64%, respectively (Figure 3). Evaluating whole SVG quantities, there were no significant difference between diseased vs. control SVGs for all parameters studied (Table 5, Figure 4). AUC values were close to 0.5, indicating inability to distinguish between diseased and control SVGs. Although LSA* was not significantly different in diseased and control SVGs, this parameter had the lowest p-value and highest AUC among all graft-averaged parameters studied (Table 5).

### Distribution of Wall Shear Stress in Diseased and Control Segments

Figure 5 shows distribution of WSS* in three representative patients. The diseased segment had notable regions of low WSS* compared to the control segments. For example, in Patient A, stenoses were located in the SVGs to the OM and RCA branches and had low WSS*, whereas the matched segment in the control SVG to diagonal branch had high WSS*. By comparison, in Patient B the stenosis was located in the SVG to the diagonal branch and had low WSS*, whereas SVGs to the OM and RCA branches had high WSS*. These qualitative maps highlighted that stenoses tended to form in regions of low WSS* irrespective of the target vessel. Patient C also supports these observations since the stenosed segment in the SVG to the OM had notably lower WSS* compared to the control segment in the SVG to the Ramus.

### Assessment of Wall Shear Stresses in the Post-Stenotic Region

To better elucidate the impact of shear forces on SVG disease, we evaluated available follow up images of the 15 patients included in our cohort. We identified a single patient

who showed a complete occlusion of a previously diseased SVG at one year follow up (Figure 6). We performed CFD simulation of the stenosed SVG and qualitatively correlated WSS* with plaque visualized on follow up CTA. We made three observations: i) calcified plaque on follow up CTA co-localized with the regions of low WSS and stenosis, iii) the region immediately distal to the stenosis had extremely low WSS, and iii) the same region presented with expansive remodelling. The WSS in this post-stenotic region was 1 dyne/$cm^2$, which was nearly 10 times lower than the graft-averaged value in that SVG.

## DISCUSSION

We have presented a detailed investigation of the role of shear stress in SVG disease using patient-specific CFD simulations. Our study offers two main findings: i) stenosis formation in SVG disease is associated with low normalized WSS in those regions, ii) SVG-averaged hemodynamics and anatomic parameters are similar between diseased and control SVGs. Our study is unique for several reasons. First, our study is the first to analyze anatomic parameters in conjunction with shear stress in patients with SVG disease. Since anatomy and hemodynamics are often corelated, the incremental value of CFD-derived parameters must be assessed against clinically-available anatomic parameters. Because we constructed anatomic models from CTA images, we were able to simultaneously characterize the SVG geometry through standard anatomic measures (e.g. area) and “hemodynamically-informed” anatomic measures (e.g. curvature, tortuosity). Second, the majority of previous studies using comparable CFD methods were exploratory and typically limited to three or fewer patients[19–21]. Of the few prior investigations with study sizes comparable to the present study, albeit different study objectives, all had major modelling limitations: i) geometric uncertainties due to X-ray angiogram reconstruction[22], ii) lack of proximal and distal vasculature[23,24], iii) non-patient-specific flow rates, and iv) low spatial and temporal resolutions on the order of 1 million tetrahedral elements and 100 time-steps per cardiac cycle, respectively[19,20,22,23]. In contrast, our CFD models were segmented directly from CTAs without any prior reconstruction, included detailed aortic and coronary branches, used echocardiography-derived inputs to ensure patient-specific conditions, and had higher spatial and temporal resolution than most prior studies. These improved methodological techniques likely resulted in more accurate shear stress predictions. Lastly, we have proposed a novel WSS normalization approach that is robust to flow rate assumptions. Flow distribution in healthy patients is typically assumed to follow known morphometric laws but may no longer remain valid in the presence of prior infarction or collateral flow and can vary substantially among patients. In the absence of advanced imaging techniques, such as coronary perfusion CTA, these assumptions are necessary but can lead to uncertainties in WSS values. To suppress the effect of this assumption, we normalized the CFD-derived WSS by its analytical WSS counterpart. The analytical WSS was obtained by assuming a straight cylinder with graft flow and diameter. Similar normalization approaches have previously been applied in other vascular territories and shown to have improved the predictive accuracy of WSS[25–27]. In our study, normalized WSS identified regions of locally low and high WSS with statistical confidence, in reference to a straight idealized “SVG” and allowed for inter- and intra-patient comparisons. The non-normalized values showed similar trends, with lower WSS in diseased grafts; however, the differences were not

statistically significant. This is likely because local differences in WSS, which are linked with focal sites of SVG disease, were washed out when averaged along the entire graft. The normalization of WSS therefore provides a useful "pseudo-geometrical" parameter that could be obtained from less comprehensive simulation strategy; however, to study vein graft mechanobiology and growth and remodeling process, we would ultimately need more comprehensive boundary conditions to obtain absolute WSS and local hemodynamic conditions.

### Relationship to Prior Studies of Wall Shear Stress in Saphenous Vein Grafts

The nominal WSS value for all SVGs in our cohort was 9 dynes/cm$^2$. A recent study of 20 patients with coronary angiography follow up at 10 year estimated WSS from thrombolysis in myocardial infarction (TIMI) frame count and analytical equation[28]. From their data, we estimated the nominal WSS in their cohort to be 13.4 dynes/cm$^2$, which is comparatively higher than 9 dynes/cm$^2$ in our study. Akasaka et al. used Doppler wire to measure flow and diameter in SVG to LAD in 13 patients at one year after CABG, which were 0.97 mL/s and 0.34 cm respectively. Based on these values, we estimated analytical WSS of 9 dynes/cm$^2$, which is identical to our CFD-derived values[29]. In contrast, Shimizu et al. estimated WSS of 5 dynes/cm$^2$ in 34 stenosed SVGs using Doppler wire four years post-CABG[30]. The comparatively lower WSS values in their study could be attributed to selection bias since all SVGs had clinically significant stenosis. Due to uncertainties attributed to various experimental approaches, a nominal WSS value in SVGs is difficult to determine but likely falls within the range of 5 to 13 dynes/cm$^3$.

The variation in the CFD literature appears to be less than in-vivo studies. A prior CFD study from our group reported WSS of 7.5 ± 3.2 dynes/cm$^2$ in seven SVGs using detailed CTA-derived models[31]. In contrast, Meirson et al. constructed 3D models from coronary angiograms and only included the SVG geometry in their CFD simulations[22]. In 50 SVGs studied, the authors reported WSS value of ~9 dynes/cm$^2$, which is identical to our study. They assigned input flow rates using TIMI frame count whereas we derived our inputs from echocardiography and clinical parameters. Despite differences in imaging modalities and modelling approaches, our WSS results were consistent with these two prior studies.

### Association Between Wall Shear Stress and Saphenous Vein Graft Disease

All of the previous studies have focused on whole graft hemodynamics; however, our findings demonstrated no significant difference in WSS between diseased and control whole SVGs. This finding is not surprising since average WSS in SVG is mainly determined by average diameter and flow rate, both of which were similar between the two groups. Our findings, however, highlighted differences in local hemodynamic conditions, which should be explored prospectively in future investigations.

Meirson et al. explored intra-patient differences in CFD-derived WSS between externally-stented versus non-stented SVGs at 1-year post-CABG[22]. Similar to our study, they found no association with WSS; they did however show OSI to be significantly higher in non-stented SVGs. This significant correlation with OSI was surprising because high OSI *alone* has not shown to be an instigator of vascular disease. Indeed, the seminal study of Ku et al.

which first introduced OSI as a biomarker showed a correlation between intimal thickness in postmortem human arteries and both high OSI *and* low WSS[32].

A recent study by Koszegi et al. estimated intra-patient differences in diseased and control SVGs using flow rates estimated from TIMI frame counts[28]. Unlike previous and present CFD studies, the authors did find a significant difference between the two groups, with values of 11.2 ± 4.2 dynes/cm$^2$ in the diseased and 15.5 ± 5 dynes/cm$^2$ in the control SVG in the same patient[28] (p=0.017). Using a threshold of 10.9 dynes/cm$^2$, the authors estimated a low sensitivity of 52% but a relatively higher specificity of 86%, which is consistent with our observations that graft-level absolute WSS may not be highly predictive of site-specific lesions.

## Mechanism of Shear Stress-Induced Wall Remodelling and SVG Disease

While abrupt increase in intramural stresses and strains contribute to intimal hyperplasia and thrombosis in the short term post implantation[33], abnormal hemodynamic conditions such as WSS and OSI, lead to atherosclerosis in the arterialized SVG in the long-term[34]. Since the interval between CTA imaging and post-CABG in our patient cohort was 10 ± 6 years (Table 2), SVG disease was likely in the atherosclerotic phase.

Our study demonstrated that SVG segments that developed stenosis had significantly lower WSS compared to control segments. Low WSS is known to promote atherosclerosis development through loss of endothelial cell alignment in the direction of the flow, increase in low-density lipoprotein cholesterol accumulation, and transmigration of macrophages, which lay the foundation of atherosclerotic plaque formation. Subsequently, there is adhesion of platelets and leukocytes and increase in expression of adhesion molecules. The process of atherosclerotic plaque formation progresses, and ultimately leads to a significant intraluminal stenosis. The presence of an intraluminal stenosis can further exacerbate the situation and initiate positive feedback leading to complete occlusion. A severe stenosis can induce regions of stagnant flow[35] and extremely low WSS immediately downstream that can be detrimental to endothelial cell function. While it is currently unknown what factors contribute to expansive or constrictive luminal remodelling, observational studies suggest that the severity of endothelial degradation and excessive expansive remodelling is significantly associated with the magnitude of low WSS[36], which is consistent with our observation of expansive remodeling in the low WSS post-stenotic region (Figure 6). Interestingly, Chatzizisis et al. demonstrated in a histopathology study of animal models that coronary regions with very low WSS, less than 5 dynes/cm$^2$, showed characteristics of high-risk plaques compared to low, intermediate and high WSS regions[36]. In these regions, those authors reported enhancement of local lipid accumulation, inflammation and oxidative stresses that promoted degradation of intima and culminated in expansive remodeling. In CABG patients, additional systematic risk factors (e.g hyperlipidemia, hypertension) and genetic factors could also interplay with low WSS to modulate the characteristics and extent of SVG disease.

## A Multi-Factorial Perspective: Incorporating Biological Response through Growth and Remodelling

Since SVGs experience substantially higher pressure and flow conditions compared to their native environment, the failure mechanism is multi-factorial and coupled, involving both shear- and intramural-stress related changes to the wall structure[37]. Although CFD modelling is able to quantify the mechanical environment, to comprehensively assess the pathophysiology of SVG disease, one would need to incorporate growth and remodeling (G&R) behaviour that integrates cellular-level details into mechanics-based models. Interestingly, our prior study using a venous G&R framework showed that a gradual rather than sudden increase in pressure and flow led to decreases in venous maladaptations[37]. We anticipate that findings from this study would allow for more precise tuning of G&R models, for example by integrating a WSS* threshold to determine constrictor or dilator concentrations, and ultimately lead to predicting long-term SVG remodeling and maladaptation in individual patients.

## Clinical Implications

Despite advances in the medical management of atherosclerotic disease, SVG failure remains prevalent and is associated with increased morbidity. Data suggest that nuclear stress testing after a mean of 7.1 years post-CABG does risk-stratify patients, but by this point many patients have advanced and irreversible SVG disease. Hence, the role of stress testing in patients after CABG is uncertain. A number of clinical and operative risk factors have been associated with increased risk of SVG failure[38], but there are currently no patient-specific tools. CFD modeling has gained recent attention with the FDA approval of HeartFlow's $FFR_{CT}$ (fractional flow reserved derived from CTA) technology and recent clinical trials demonstrating significant correlation with invasive FFR. However, no analogous technology exists to identify CABG patients who are at increased risk of SVG disease after CABG. Using detailed CFD modeling, in this pilot study we found that low WSS was associated with late-stage SVG disease, although a larger prospective clinical trial is necessary to validate our findings. If patients could be identified early who are at increased risk of SVG failure, they may benefit from more intensive medical therapy and/or from increased surveillance to identify early SVG disease and possible percutaneous interventions as needed to maintain graft patency.

## Strengths and Limitations

A major strength of our study was that we selected patients as their own controls. This approach allowed matched pairs of SVGs that were identical in all potential systemic confounders and only differed in local flow parameters. Another strength was that we used detailed CTA models and inputs from echocardiography that allowed for patient-specific hemodynamic computations. Lastly, although our cohort size is relatively small, this is the largest and most well-defined CFD study to investigate SVG disease.

A key limitation was that we lacked prospective data, and thus, had to virtually reverse the stenosis to approximate pre-diseased conditions. While our virtual reversal may not have accurately captured the immediate post-CABG anatomy, it likely is a good approximation of the pre-diseased state. Since there is a lack of literature on coronary flow distribution

in post-CABG patients, our boundary conditions were based on literature data of healthy volunteers, which may add uncertainty to the predicted flow rates. However, in spite of this limitation, our vein graft flow rates of 0.75 ± 0.39 ml/s compared reasonably to previously reported doppler-measured flow rates of 1 ± 0.3 ml/s in SVGs to the LAD[29]. Even though the pathophysiological mechanisms of graft failure are not completely understood, it is known that the interplay between local hemodynamics and vascular biology determines long-term outcome of the graft. Our CFD models lack the cellular and sub-cellular scales needed to capture the evolving nature of SVG adaptation and work in this direction is ongoing.

## CONCLUSIONS

We presented the first detailed CFD study to characterize hemodynamic and anatomic parameters in CABG patients who developed SVG stenosis. We found a significant difference in normalized WSS in local SVG regions that developed stenosis compared to control segments. We found no significant difference in whole SVG hemodynamic and anatomic parameters. Our study is a crucial step towards developing CFD-based predictive strategies to identify high-risk post-CABG patients who may benefit from improved medical management and closer follow-up.

## ACKNOWLEDGEMENTS

The authors wish to thank Derrick Laurel from the 3D and Quantitative Imaging Laboratory for his help in constructing models from CTA data, and Dr. Jin Long at the Quantitative Science Unit at the Stanford University School of Medicine for his help in statistical analysis.

SOURCES OF FUNDING

This work was supported by NIH grant (NIH R01-RHL123689A), NSF CAREER Award OCI-1150184 to A. L. M., and a Burroughs Wellcome Fund Career Award at the Scientific Interface to A. L. M. Computational resources were provided by a grant to A. L. M (TG-CTS130034) through the Extreme Science and Engineering Discovery Environment (XSEDE). R.R.S.P. is supported by VA Merit BX004558. M. O. K. acknowledges funding support from the Natural Sciences and Engineering Research Council of Canada.

## REFERENCES

1. D'Agostino RS, Jacobs JP, Badhwar V, et al.The Society of Thoracic Surgeons Adult Cardiac Surgery Database: 2019 Update on Outcomes and Quality. Ann Thorac Surg. 2019;107(1):24–32. doi:10.1016/j.athoracsur.2018.10.004 [PubMed: 30423335]
2. Goldman S, Zadina K, Moritz T, et al.Long-term patency of saphenous vein and left internal mammary artery grafts after coronary artery bypass surgery. JACC Cardiovacular Interv. 2004;44(11):2149–2156. doi:10.1016/j.jacc.2004.08.064
3. Hess CN, Lopes RD, Gibson CM, et al.Saphenous vein graft failure after coronary artery bypass surgery insights from PREVENT IV. Circulation. 2014;130(17):1445–1451. doi:10.1161/CIRCULATIONAHA.113.008193 [PubMed: 25261549]
4. Weintraub WS, Jones EL, Morris DC, King SB, Guyton RA, Graver JM. Outcome of reoperative coronary bypass surgery versus coronary angioplasty after previous bypass surgery. Circulation. 1997;95(4):868–877. doi:10.1161/01.CIR.95.4.868 [PubMed: 9054744]
5. De Vries MR, Simons KH, Jukema JW, Braun J, Quax PHA. Vein graft failure : from pathophysiology to clinical outcomes. Nat Rev Cardiol. 2016;13(8):451–470. doi:10.1038/nrcardio.2016.76 [PubMed: 27194091]

6. Malek A, Alpher S, Izumo S. Hemodynamic shear stress and its role in atherosclerosis. JAMA. 1999;282(21):2035–2042. [PubMed: 10591386]
7. Markl M, Frydrychowicz A, Kozerke S, Hope M, Wieben O. 4D Flow MRI. J Magn Reson Im. 2012;36:1015–1036. doi:10.1002/jmri.23632
8. Morris PD, Narracott A, Von Tengg-Kobligk H, et al.Computational fluid dynamics modelling in cardiovascular medicine. Heart. 2016;102(1):18–28. doi:10.1136/heartjnl-2015-308044 [PubMed: 26512019]
9. Lu MT, Ferencik M, Roberts RS, et al.Noninvasive FFR Derived From Coronary CT Angiography - Management and outcomes in the PROMISE Trial. JACC Cardiovasc Imaging. 2017;10(11):1350–1358. doi:10.1016/j.jcmg.2016.11.024 [PubMed: 28412436]
10. Packard RRS, Li D, Budoff MJ, Karlsberg RP. Fractional flow reserve by computerized tomography and subsequent coronary revascularization. Eur Heart J Cardiovasc Imaging. 2017;18(2):145–152. doi:10.1093/ehjci/jew148 [PubMed: 27469588]
11. Sankaran S, Moghadam ME, Kahn AM, Tseng EE, Guccione JM, Marsden AL. Patient-specific multiscale modeling of blood flow for coronary artery bypass graft surgery. Ann Biomed Eng. 2012;40(10):2228–2242. doi:10.1007/s10439-012-0579-3 [PubMed: 22539149]
12. Tran JS, Schiavazzi DE, Ramachandra AB, Kahn AM, Marsden AL. Automated tuning for parameter identification and uncertainty quantification in multi-scale coronary simulations. Comput Fluids. 2016;142:128–138. doi:10.1016/j.compfluid.2016.05.015 [PubMed: 28163340]
13. Ramachandra AB, Kahn AM, Marsden AL. Patient-Specific Simulations Reveal Significant Differences in Mechanical Stimuli in Venous and Arterial Coronary Grafts. J Cardiovasc Transl Res. 2016;9(4):279–290. doi:10.1007/s12265-016-9706-0 [PubMed: 27447176]
14. Gaudino M, Antoniades C, Benedetto U, et al.Mechanisms, consequences, and prevention of coronary graft failure. Circulation. 2017;136(18):1749–1764. doi:10.1161/CIRCULATIONAHA.117.027597 [PubMed: 29084780]
15. Podesser BK, Neumann F, Neumann M, Schreiner W, Wollenek G, Mallinger R. Outer radius-wall thickness ratio, a postmortem quantitative histology in human coronary arteries. Acta Anat (Basel). 1998;163(2):63–68. [PubMed: 9873135]
16. Johnson K, Sharma P, Oshinski J. Coronary artery flow measurement using navigator echo gated phase contrast magnetic resonance velocity mapping at 3.0 T. J Biomech. 2008;41(3):595–602. doi:10.1016/j.jbiomech.2007.10.010 [PubMed: 18036532]
17. Zamir M, Sinclair P, Wonnacott TH. Relation between diameter and flow in major branches of the arch of the aorta. J Biomech. 1992;25(11):1303–1310. doi:10.1016/0021-9290(92)90285-9 [PubMed: 1400531]
18. Changizi MA, Cherniak C. Modeling the large-scale geometry of human coronary arteries. Can J Physiol Pharmacol. 2000;78(8):603–611. [PubMed: 10958160]
19. Zhao X, Liu Y, Li L, Wang W, Xie J, Zhao Z. Hemodynamics of the string phenomenon in the internal thoracic artery grafted to the left anterior descending artery with moderate stenosis. J Biomech. 2016;49(7):983–991. doi:10.1016/j.jbiomech.2015.11.044 [PubMed: 26972762]
20. Zhao Z, Mao B, Liu Y, Yang H, Chen Y. The Study of the Graft Hemodynamics with Different Instant Patency in Coronary Artery Bypassing Grafting. Comput Model Eng Sci. 2018;116(2):229–245. doi:10.31614/cmes.2018.04192
21. Dur O, Coskun ST, Coskun KO, Frakes D, Kara LB, Pekkan K. Computer-Aided Patient-Specific Coronary Artery Graft Design Improvements Using CFD Coupled Shape Optimizer. Cardiovasc Eng Technol. 2011;2(1):35–47. doi:10.1007/s13239-010-0029-z [PubMed: 22448203]
22. Meirson T, Orion E, Di Mario C, et al.Flow patterns in externally stented saphenous vein grafts and development of intimal hyperplasia. J Thorac Cardiovasc Surg. 2015;150(4):871–878. doi:10.1016/j.jtcvs.2015.04.061 [PubMed: 26242834]
23. Fan T, Feng Y, Feng F, et al.A comparison of postoperative morphometric and hemodynamic changes between saphenous vein and left internal mammary artery grafts. Physiol Rep. 2017;5(21):1–12. doi:10.14814/phy2.13487
24. Ballarin F, Faggiano E, Manzoni A, et al.Numerical modeling of hemodynamics scenarios of patient-specific coronary artery bypass grafts. Biomech Model Mechanobiol. 2017:1–27. doi:10.1007/s10237-017-0893-7

25. Khan M, Valen-Sendstad K, Steinman D. Narrowing the expertise gap for predicting intracranial aneurysm hemodynamics: Impact of solver numerics versus mesh and time-step resolution. AJNR Am J Neuroradiol. 2015;36:1310–1316. doi:10.3174/ajnr.A4263 [PubMed: 25742983]
26. Xiang J, Natarajan S, Tremmel M, et al.Hemodynamic-morphologic discriminants for intracranial aneurysm rupture. Stroke. 2011;42(1):144–152. doi:10.1161/STROKEAHA.110.592923 [PubMed: 21106956]
27. Khan MO, Arana VT, Rubbert C, et al.Association between aneurysm hemodynamics and wall enhancement on 3D vessel wall MRI. J Neurosurg. 2020:1–11. doi:10.3171/2019.10.JNS191251.
28. Koszegi Z, Kiss B, Sipos D, et al.Comparing the shear stress in degenerated and intact venous grafts from the same patients. Eur Heart J. 2018;39(Suppl_1):ehy565–P2695.
29. Akasaka T, Yoshikawa J, Yoshida K, et al.Flow capacity of internal mammary artery grafts: Early restriction and later improvement assessed by doppler guide wire. Comparison with saphenous vein grafts. J Am Coll Cardiol. 1995;25(3):640–647. doi:10.1016/0735-1097(94)00448-Y [PubMed: 7860908]
30. Shimizu T, Ito S, Kikuchi Y, et al.Arterial conduit shear stress following bypass grafting for intermediate coronary artery stenosis: A comparative study with saphenous vein grafts. Eur J Cardio-thoracic Surg. 2004;25(4):578–584. doi:10.1016/j.ejcts.2003.12.039
31. Ramachandra A, Kahn A, Marsden A. Patient-Specific Simulations Reveal Significant Differences in Mechanical Stimuli in Venous and Arterial Coronary Grafts. J Cardiovasc Transl Res. 2016:279–290. doi:10.1007/s12265-016-9706-0 [PubMed: 27447176]
32. Ku D, Giddens D, Zarins C, Glagov S. Pulsatile flow and atherosclerosis in the human carotid bifurcation. Positive correlation between plaque location and low oscillating shear stress. Arteriosclerosis. 1985;5(3):293–302. doi:10.1161/01.ATV.5.3.293 [PubMed: 3994585]
33. Hozumi T, Yoshikawa J, Yoshida K, et al.Use of intravascular ultrasound for in vivo assessment of changes in intimal thickness of angiographically normal saphenous vein grafts one year after aortocoronary bypass surgery. Heart. 1996;76(4):317–320. doi:10.1136/hrt.76.4.317 [PubMed: 8983677]
34. Motwani J, Topol E. Aortocoronary saphenous vein graft disease. Pathogenesis, predisposition, and prevention. Circulation. 1998;97(9):916–931. doi:10.4324/9781315731964-2 [PubMed: 9521341]
35. Khan M, Valen-Sendstad K, Steinman D. Direct Numerical Simulation of Laminar-Turbulent Transition in a Non-Axisymmetric Stenosis Model for Newtonian vs. Shear-Thinning Non-Newtonian Rheologies. Flow Turbul Combust. 2018.
36. Chatzizisis YS, Jonas M, Coskun AU, et al.Prediction of the localization of high-risk coronary atherosclerotic plaques on the basis of low endothelial shear stress: an intravascular ultrasound and histopathology natural history study. Circulation. 2008;117(8):993–1002. doi:10.1161/CIRCULATIONAHA.107.695254 [PubMed: 18250270]
37. Ramachandra AB, Humphrey JD, Marsden AL. Gradual loading ameliorates maladaptation in computational simulations of vein graft growth and remodelling. J R Soc Interface. 2017;14(130). doi:10.1098/rsif.2016.0995
38. Shah PJ, Gordon I, Fuller J, et al.Factors affecting saphenous vein graft patency: Clinical and angiographic study in 1402 symptomatic patients operated on between 1977 and 1999. J Thorac Cardiovasc Surg. 2003;126(6):1972–1977. doi:10.1016/S0022-5223(03)01276-5 [PubMed: 14688715]

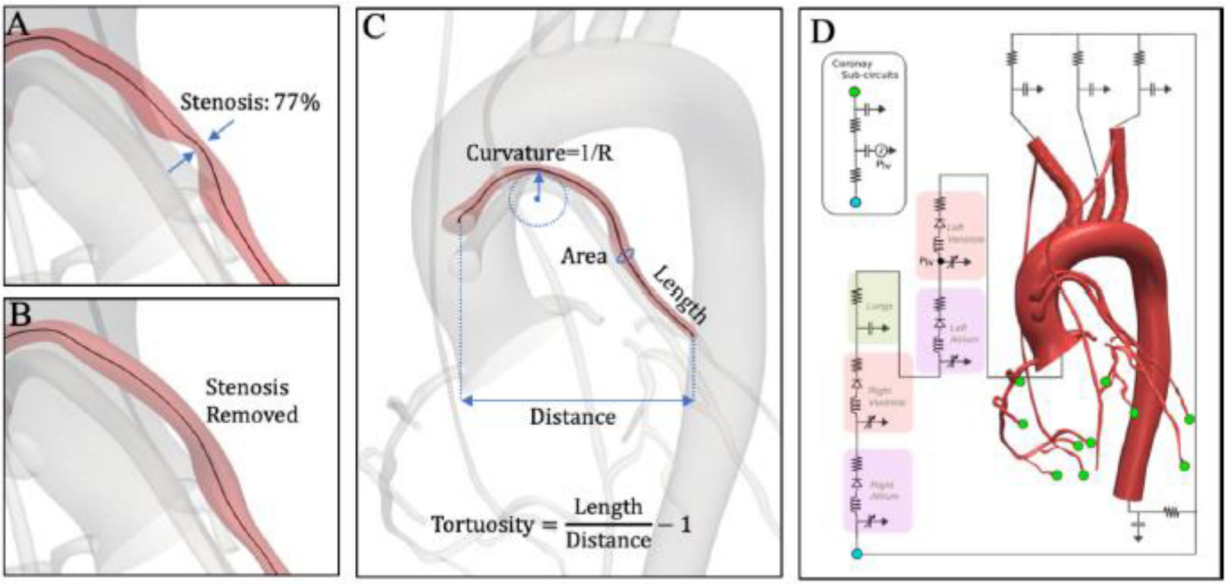


**Fig 1:**

A) Stenosis with a severity of 77% area reduction at the mid-portion of the SVG. B) Virtual removal of the stenosis to obtain pre-diseased state. C) Anatomic parameters computed from 3D models reconstructed from patients' CTA data. D) Schematic view of a multi-scale patient-specific model of the coronary circulation, coupling a closed-loop lumped parameter network (LPN) to a 3D model. The LPN parameters, such as resistances and capacitances, were tuned to match clinical targets to within 10%.

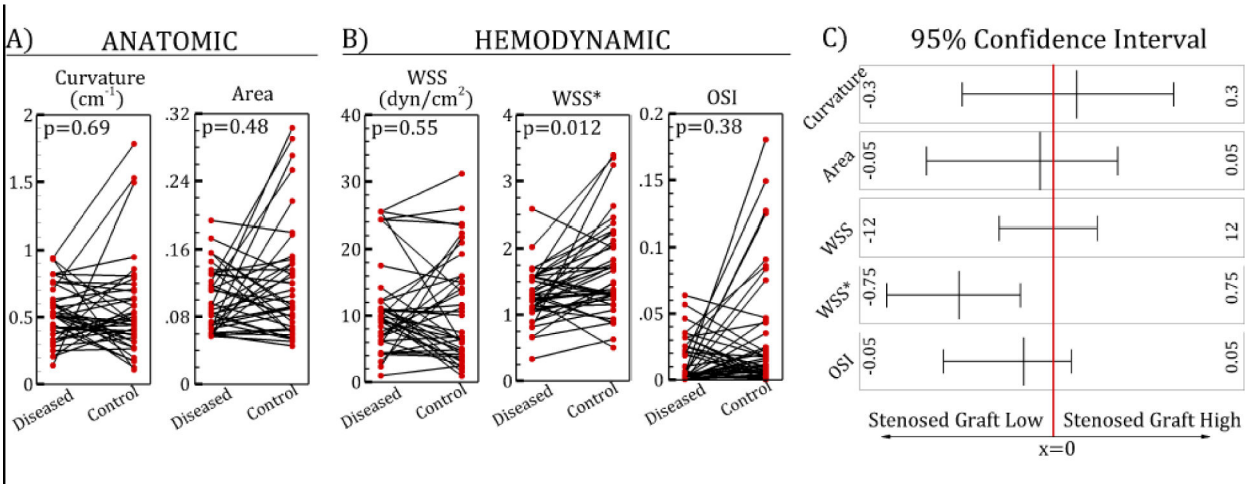


**Fig 2:**

Paired plots of anatomic (A) and hemodynamic (B) parameters of diseased vs. control saphenous vein graft (SVG) segments. (C) 95% confidence intervals. WSS, wall shear stress, WSS*, normalized wall shear stress; OSI, oscillatory shear index.

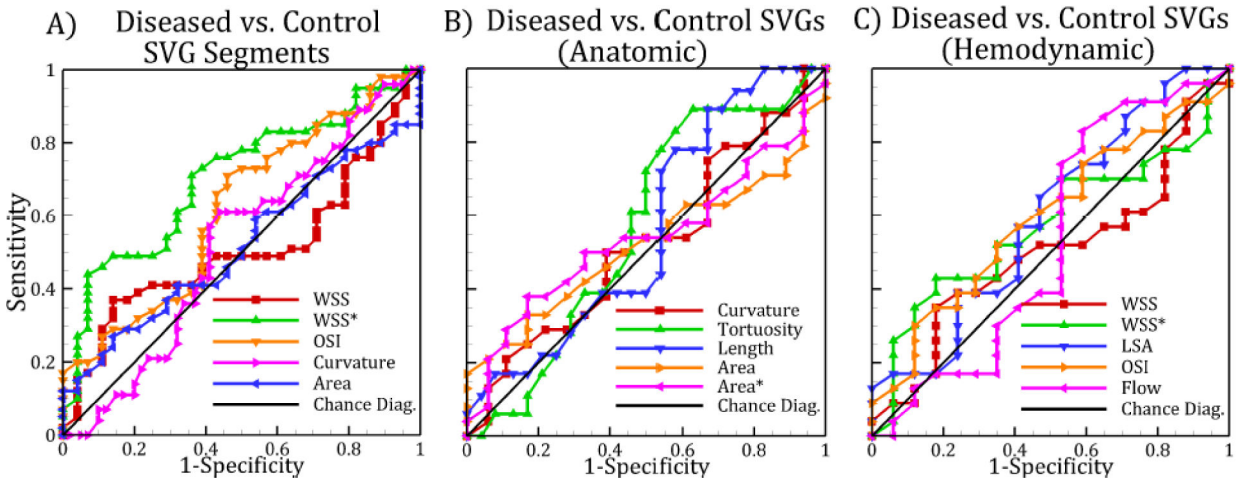


**Fig 3:**

Receiver operating characteristic (ROC) curve of local saphenous vein graft (SVG) parameters (A). ROC curve of whole SVG parameters for (B) anatomic and (C) hemodynamic parameters. The diagonal line corresponds to the line of no-discrimination. WSS, wall shear stress, WSS*, normalized wall shear stress; LSA, low shear area; OSI, oscillatory shear index.

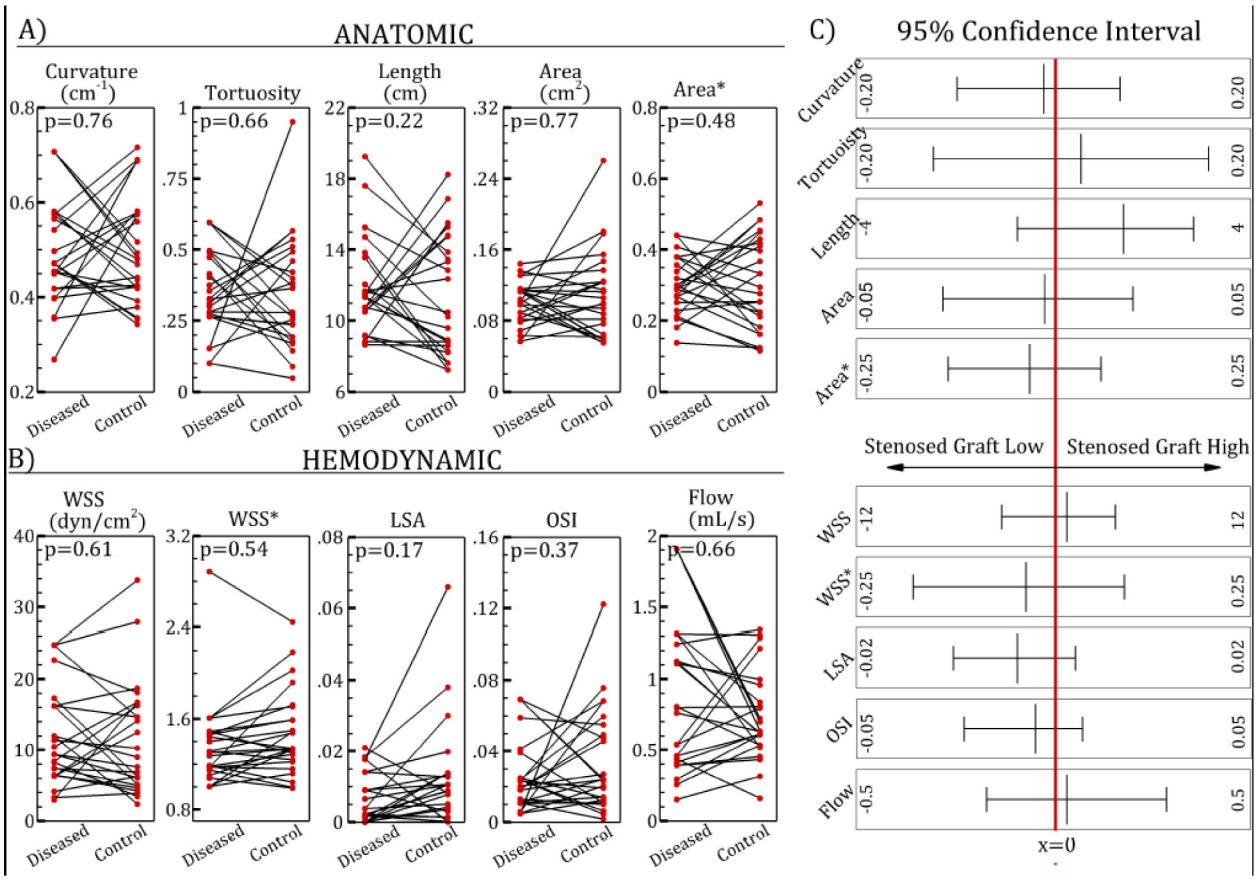


**Fig 4:**

Paired plots of anatomic (A) and hemodynamic (B) parameter of diseased and control saphenous vein grafts (SVGs). C) 95% confidence intervals. WSS, wall shear stress, WSS*, normalized wall shear stress; LSA, low shear area; OSI, oscillatory shear index.

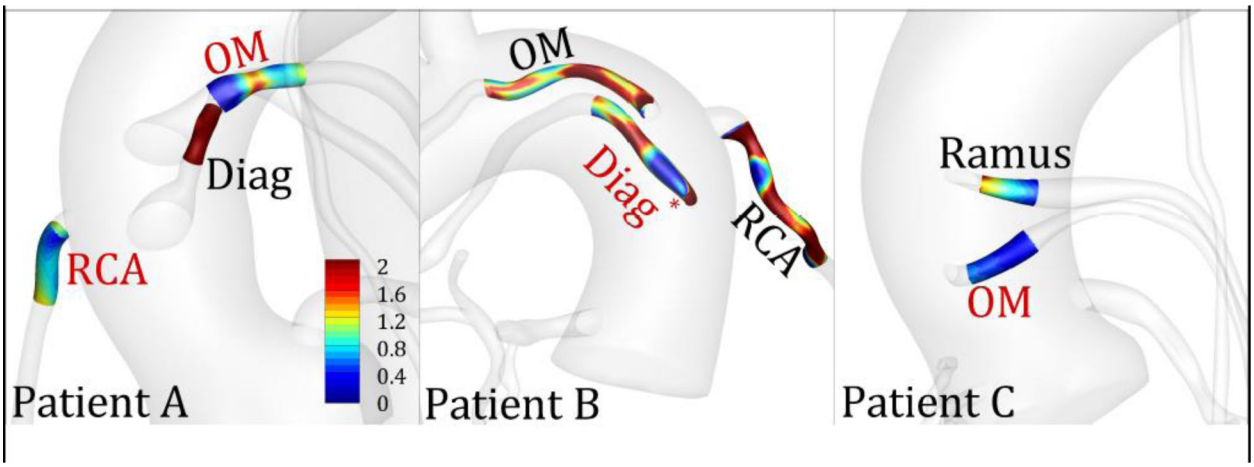


**Fig 5:**

Distribution of normalized wall shear stress (WSS*) in diseased and control segments in three representative patients. The labels indicate the target vessel to which the SVG was anastomosed. Red and black color fonts represent diseased and control segments, respectively. * indicates that the diseased region was segmented from a stent rather than a stenosis on the CTA. OM, obtuse marginal; Diag, diagonal; RCA, right coronary artery.

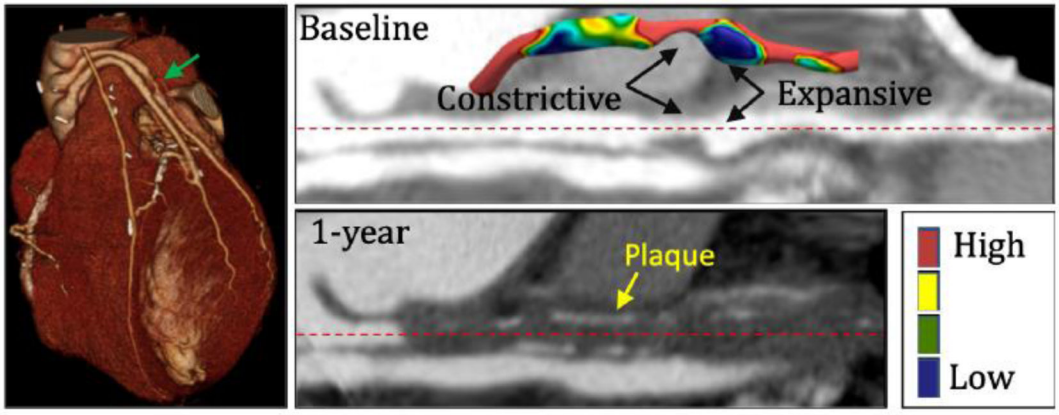


**Fig 6:**

Shear stress profile in region immediately distal to a severe stenosis. The left panel shows a 3D CTA visualization of a patient with stenosed SVG that was completely occluded at 1-year follow up. The green arrow identifies the stenosis. The right top and bottom panels show registered straightened image of the stenosed vessel at baseline and at 1-year follow, respectively. Inset in the top panel shows shear stress map of the stenosed SVG that highlights regions of very low WSS immediately downstream of the stenosis and an expansive remodeling phenomenon. Calcified plaque is visualized in the occluded SVG at 1-year follow-up and is marked with yellow arrow.

**Table 1:**

Definition of shear stress-based parameters.

| Parameter | Definition | Description |
|---|---|---|
| Wall shear stress (WSS) | $\frac{1}{T}\int_0^T \lvert\tau_w\rvert dt$ | Measure of flow-induced shear forces on the SVG wall. The values typically range from 10 – 50 dynes/cm$^2$. |
| Normalized wall shear stress (WSS*) | $\frac{WSS}{\left(\frac{32\mu Q}{\pi D^3}\right)}$ | Measure of flow-induced shear forces on the SVG wall compared to a straight pipe. $\mu$, Q and D correspond to blood viscosity, flow rate and mean graft diameter, respectively. |
| Low shear area* (LSA) | $\frac{1}{A_T}\int_0^X A_{<10\%WSS} dx$ | Measure of SVG surface area exposed to very low shear stress. |
| Oscillatory shear index (OSI)[a] | $0.5\left\{1-\frac{\left\lvert\int_0^T \tau_w dt\right\rvert}{\int_0^T \lvert\tau_w\rvert dt}\right\}$ | Measure of multi-directionality of wall shear stress. Values are bounded between 0 – 0.5. Low values indicate purely forward shear and high values indicate uniaxial wall shear stress with reversal or multi directional wall shear stress*. |

[a]OSI cannot distinguish between a uniaxial shear stress with complete reversal or multidirectional shear stress. SVG, saphenous vein graft.

**Table 2:**

Demographic and clinical characteristic of study population (n=15)

| | |
|---|---|
| Age, y | 71.5 ± 9.5 |
| Female, n (%) | 1 (7) |
| Years since CABG, y | 10 ± 6 |
| Body mass index, kg/m$^2$ | 25.2 ± 2.2 |
| Diabetes, n (%) | 7 (47) |
| Hypertension, n (%) | 14 (100) * |
| Hyperlipidemia, n (%) | 14 (100) * |
| Smoking history, n (%) | 6 (40) |
| Family history of CAD, n (%) | 11 (73) |
| Previous MI, n (%) | 14 (100) * |
| LVEF | 48% ± 15% |
| No. of SVGs per patient | 2.7 ± 0.7 |
| No. of patients with LIMA grafts | 12 (80%) |
| No. of patients with RIMA grafts | 1 (7%) |

Data are mean and standard deviation when appropriate. CAD, coronary artery disease; MI, myocardial infarction; LVEF, left ventricle ejection fraction; LIMA/RIMA, left/right internal mammary artery.

* Data for one patient was not available.

**Table 3:**

Saphenous vein graft (SVG) target vessels and patency status.

| | |
|---|---|
| Total No. of SVGs | 40 |
| • Stented/Stenosed (>60%) | 17 |
| • Non-stenosed | 23 |
| Stenosed/Stented SVG target vessel (n=17) | |
| • Diagonal, n (%) | 2 (12) |
| • OM, n (%) | 10 (59) |
| • RCA, n (%) | 5 (29) |
| Non-stenosed SVG target vessel (n=23) | |
| • LAD, n (%) | 4 (18) |
| • Diagonal, n (%) | 4 (18) |
| • OM, n (%) | 7 (30) |
| • RCA, n (%) | 7 (30) |
| • Ramus, n (%) | 1 (4) |
| No. of SVGs with stents (N=5) | |
| • Diagonal, n (%) | 2 (40) |
| • OM, n (%) | 3 (60) |

OM, obtuse marginal; RCA, right coronary artery; LAD, left anterior descending artery.

**Table 4:**

Results from univariate statistical analysis, showing median and interquartile range (IQR) for diseased vs control segments of saphenous vein grafts (SVGs). a) anatomic parameters, b) hemodynamic parameters.

| | Parameter | Diseased SVG Segment | | Control SVG Segment | | P | AUC |
|---|---|---|---|---|---|---|---|
| | | Median | IQR | Median | IQR | | |
| a | Curvature (1/cm) | 0.51 | 0.28 | 0.49 | 0.41 | 0.69 | 0.52 |
| | Area ($cm^2$) | 0.094 | 0.061 | 0.091 | 0.060 | 0.48 | 0.52 |
| | | | | | | | |
| b | WSS (dynes/$cm^2$) | 9.40 | 4.59 | 10.01 | 8.66 | 0.55 | 0.51 |
| | WSS* | 1.22 | 0.43 | 1.73 | 0.81 | 0.012† | 0.71 |
| | OSI | 0.0051 | 0.019 | 0.013 | 0.016 | 0.38 | 0.62 |

WSS, wall shear stress; WSS*, normalized wall shear stress; OSI, oscillatory shear index.

† indicates statistical significances.

**Table 5:**

Results from univariate statistical analysis, showing median and interquartile range (IQR) for diseased vs. control whole saphenous vein grafts (SVGs). a) anatomic parameters, b) hemodynamic parameters.

| | Parameter | Diseased SVG | | Control SVG | | P | AUC |
|---|---|---|---|---|---|---|---|
| | | Median | IQR | Median | IQR | | |
| a | Curvature (1/cm) | 0.46 | 0.13 | 0.47 | 0.14 | 0.76 | 0.52 |
| | Tortuosity | 0.34 | 0.13 | 0.30 | 0.20 | 0.66 | 0.57 |
| | Length (cm) | 11.59 | 3.92 | 12.39 | 5.95 | 0.22 | 0.56 |
| | Area ($cm^2$) | 0.098 | 0.032 | 0.099 | 0.063 | 0.77 | 0.52 |
| | Area | 0.29 | 0.12 | 0.31 | 0.20 | 0.48 | 0.54 |
| | | | | | | | |
| b | WSS (dynes/$cm^2$) | 8.37 | 5.56 | 9.00 | 10.40 | 0.61 | 0.50 |
| | WSS* | 1.27 | 0.27 | 1.34 | 0.42 | 0.54 | 0.57 |
| | LSA* | 0.0038 | 0.0090 | 0.0081 | 0.011 | 0.17 | 0.60 |
| | OSI | 0.019 | 0.014 | 0.024 | 0.035 | 0.37 | 0.60 |
| | Flow (mL/s) | 0.76 | 0.71 | 0.63 | 0.32 | 0.66 | 0.53 |

WSS, wall shear stress; WSS*, normalized wall shear stress; LSA*, low shear area; OSI, oscillatory shear index.